

Shear-induced particle migration in one-, two-, and three-dimensional flows

C. Gao and J. F. Gilchrist*

Department of Chemical Engineering, Lehigh University, Bethlehem, Pennsylvania 18015, USA

(Received 19 October 2007; published 7 February 2008)

We investigate the segregation resulting from the competition between advection and shear-induced migration of suspensions in steady open flows. Herringbone channels form a concentration profile deviating from the particle focusing found in straight channels. Transients can result from a buckling instability during the onset of migration when particle-depleted fluid is injected into particle-rich fluid. In chaotic flows, the better mixing found at low bulk volume fraction is not seen at higher bulk volume fraction. Thus, the ability of static mixers to reduce the effects of shear-induced migration is significantly limited.

DOI: [10.1103/PhysRevE.77.025301](https://doi.org/10.1103/PhysRevE.77.025301)

PACS number(s): 47.57.-s, 47.52.+j, 47.61.Ne

It is well known that particles in a flow do not passively follow along fluid streamlines. For example, multibody hydrodynamic interactions can lead to shear-induced migration, a phenomenon that has received significant attention since its first detailed description by Leighton and Acrivos [1]. Shearing of fluids having a significant volume fraction of solid particles leads to cross-streamline migration, resulting in higher local concentrations in regions of low shear. In a Poiseuille flow, this drives particles from the walls to the center of the channel. The local increase in viscosity as a result of this migration acts as a feedback mechanism, blunting the velocity profile and increasing the local shear rate near the walls. The final steady profile is achieved when particles are redistributed such that the suspension stresses are once again balanced. This occurs far from the entrance conditions, scaling as $\frac{L}{H} \sim \frac{1}{f(\phi)} \left(\frac{H}{a}\right)^2$, where L and H are the length and half-height of the channel, respectively, a is the particle radius, and $f(\phi)$ is related to the short-time collisional diffusivity, $D_c = f(\phi) \dot{\gamma} a^2$ [1,2]. While details differ between migration of Brownian and non-Brownian particles, the general result is similar for flows at high Péclet number, $Pe \equiv \frac{6\pi\eta_0\dot{\gamma}a^3}{kT}$ for shear rate $\dot{\gamma} = \frac{v_{max}}{H}$.

Shear-induced migration has been investigated primarily in systems that generate one-dimensional (1D) flows, where $\bar{v} = f(x_1)$ such as Poiseuille flows [3–8] and Couette cells [9–12], primarily to understand its effect on rheological measurements. More recently, studies have investigated 2D systems, including sudden contractions and expansions [13–15], and steady 2D closed flows [16–18]. These systems differ significantly from 1D flows because of the way the normal stresses interplay with the orientation of the local shear. Like 1D flows, 2D flows where $\bar{v} = f(x_1, x_2)$ have the constraint of closed streamlines, still a reduced level of complexity not typically found in industrial or natural systems. With more complicated particulate species such as long-chain polymers [19], DNA [20], or cells [21], migration can occur as the result of coupled hydrodynamic and elastic interactions.

It has long been shown that 2D time-periodic and 3D steady flows $\bar{v} = f(x_1, x_2, T_n < t < T_{n+1})$ and $\bar{v} = f(x_1, x_2, x_3)$, respectively, can result in chaotic advection [22]. This has been

proven to be significant in enhancing mixing and transport rates at low Reynolds numbers. Chaotic advection typically results from breaking the symmetries in the flow to repeatedly stretch and fold fluid elements until striations are of length scales where diffusive processes dominate. Recently, issues of poor transport in microchannels have been overcome by introducing either time periodicity and/or geometric perturbations to induce chaotic advection [23]. Studies of the mixing performance of these channels focus on Newtonian fluids; however, many microscale systems manipulate dilute to moderately concentrated suspensions.

The primary question explored in this Rapid Communication is, what is the interplay between shear-induced migration and advection in the transverse direction producing 2D and 3D (chaotic) advection? More pointedly, which dominates—self-organization or dispersion? We investigate this competition in suspensions of monosized 1- μm silica microspheres in steady pressure-driven flows in microchannels generating flow topologies ranging from simple unidirectional and integrable to complicated velocity profiles exhibiting chaotic advection.

The microchannels used in this study are similar to herringbone (HB) channels fabricated by Stroock *et al.* [24] to study chaotic mixing at small scales. They found that the angled recesses along one wall of the channel produce recirculation in the transverse (y - z) direction to the primary flow in the x direction for Newtonian fluids. The geometries used in this study, fabricated using polydimethylsiloxane soft lithography [25], are depicted in Fig. 1(A). The primary channel flow path is $W \times H \times L$ of $90 \mu\text{m} \times 30 \mu\text{m} \times 30 \text{mm}$. Fluid moves inward near the top of the channel and outward near the bottom, and the local separatrix that divides the two resulting vortices is located at the tip of the HB, either in the center for 2D flows or offset from the center by alternating left and right every 6 HBs. The suspension consists of $2a = 1.01 \mu\text{m}$ monosized microspheres at volume fractions $\phi_{bulk} = 0.1$ and 0.2 in a 3:1 glycerin:water mixture ($\eta_0 = 0.04 \text{ Pa s}$, $\rho = 1.20 \text{ g/cm}^3$) to partially index-match the fluid to the microspheres. The solution is adjusted to $pH = 8.0$ and 0.025 mM NaNO_3 to produce a Debye screening length $\kappa^{-1} = 1.5 \text{ nm}$ on the charge-stabilized microspheres and $0.1 \text{ mM Rhodamine B}$ is added for imaging. Flow is pressure driven by a syringe pump (Harvard Apparatus) resulting in a maximum velocity of $200 \mu\text{m/s}$, as determined by velocim-

*gilchrist@lehigh.edu

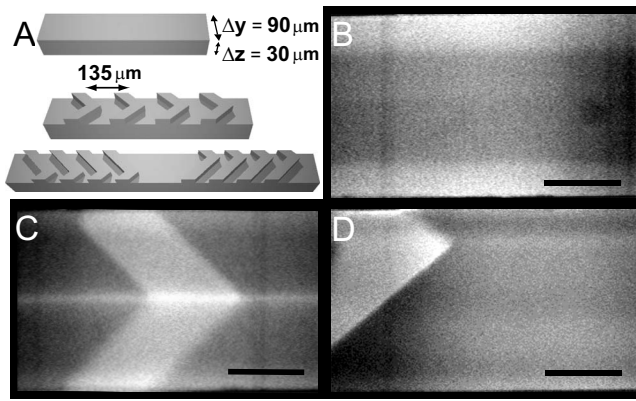


FIG. 1. (A) A schematic diagram of the geometries of the microchannels that generate 1D, 2D, and 3D flows. The experimental images below show the relative concentration where darker areas are regions of higher particle concentration; the scale bar is $40 \mu\text{m}$. (B) Straight channels demonstrate classic shear migration, concentrating particles in the center of the channel. (C) Recirculation in the transverse direction does not mediate shear-induced migration, generating two side-by-side segregated regions where particles migrate away from the center of the channel. (D) A 3D chaotic flow that demonstrates chaotic advection results in multiple dark bands, two near the walls and one near the center of the channel.

etry, at $\text{Pe}=5100$ and $\text{Re}=8.2 \times 10^{-7}$ ($\text{Re} \equiv \frac{\rho a^2 \dot{\gamma}}{\eta_0}$). Final patterns in these geometries have been studied up to $\text{Pe}=1.2 \times 10^5$ ($\text{Re}=2 \times 10^{-5}$) and are general at the high-Pe and low-Re limit.

The initial concentration profile cannot be prescribed exactly; any shear within the connections leading to the main channel leads to particle migration. To mediate the effects of migration, the connection from the tube to the device is a 90° bend and the entrance to the channel is tapered with a 15° restriction to avoid jamming and yet force particles toward the walls. Thus, the initial concentration is mostly uniform at the channel entrance with the exception of one to two particle diameters distance from the walls, where shear is highest and particle volume exclusion occurs regardless of migration. At $\phi_{\text{bulk}}=0.1$, particles are on average separated by less than $2a$. Volume fractions significantly less than this do not generate normal forces sufficient to result in significant migration [26]. The particles are not neutrally buoyant. In this study $\Delta\rho=0.8 \text{ g/cm}^3$, which leads to a slight migration downward in the z direction, primarily observed at $\phi = 0.1$ in the bottom corners. This profile is similar to previous studies of resuspension [27]; however, no significant secondary flows are evident in the straight channels.

The straight HB and staggered herringbone (SHB) mixers shown in Fig. 1(A) define 1D, 2D, and 3D flows. In the 1D flow [Fig. 1(B)], fluid streamlines are solely parallel to the axial direction (x direction) of the channel. Typical of pressure-driven flow, the fastest velocity and lowest shear rate is located in the center of the channel. Far from the entrance, at $\frac{L}{H}=2000 > \left(\frac{H}{a}\right)^2=900$ [28], the fluorescence image of the 1D suspension flow shows the steady concentration profile after migration drives particles from the walls toward the center of the channel, similar to previous studies [3–7].

In the 2D flow [Fig. 1(C)] generated by the HB geometry, mixing of Newtonian fluids is enhanced but still linear, where fluid elements are confined to side-by-side toroidal regions spanning the length of the channel. In the transverse direction, the flow is split into two recirculating vortices with fluid moving downward in the center and upward at the walls as a result of the boundary condition at the top surface of the channel. The resulting segregation profile of the suspension in this geometry shows that particles migrate away from the center of the channel. Like the 1D flow, particles migrate away from the walls as expected due to the locally high shear rate. The suspension focuses into two bands, and the concentration gradient aligns roughly normal to the closed manifolds created of the two vortices generated by this geometry. This sharp concentration gradient at the centerline is a result of recirculation of fluid from the particle-depleted fluid in the near-wall region resulting from near-wall particle exclusion and shear-induced migration.

In the SHB channel [Fig. 1(D)], the flow shown generates three regions of higher particle concentration, two located by the walls and one twisting through the middle of the channel. Once again, deviation from forming a single straight band of concentrated particles is due to the interplay of shear migration and the underlying flow. This geometry [24] generates weakly chaotic 3D flows in Newtonian fluids having coexisting regions of exponential rates of mixing due to chaotic advection and toroidal regions of integrable trajectories having linear rates of mixing bound by KAM surfaces that act as barriers to advective transport [22]. For suspensions, it is speculated that these regions of relatively poor mixing will interplay with the formation of segregated bands. It must be noted that the final segregation profile in various experiments is not identical, where the evolution of the coarsening of these concentration gradients likely depends strongly on the initial concentration profile and subtle differences in imperfections residing in microfabricated channels.

While profiles shown by a single vantage point viewed in the z direction give many details of the concentration profiles, these do not necessarily represent the internal segregation structure; nor do they quantify the degree of shear-induced migration. Figure 2 shows the quantitative transverse concentration profiles in 1D, 2D, and 3D flows [29]. Edges of the channel, where slowly moving particles inaccurately represent the local concentration, have been clipped uniformly. In 1D flows, the concentrated band of particles is shown to have segregated both from the side walls and the top and bottom surfaces in both $\phi_{\text{bulk}} = 0.1$ and 0.2 . The region of highest concentration is located roughly equidistant from the boundaries, where its shape is loosely defined by curves of constant shear rate, directly related to the stress defining the degree of shear migration. The maximum concentration of $\phi=0.16$ and $\phi=0.275$ and the shape of the profile in the z direction agree well with previous studies at similar concentrations and Pe [5]. The gradients of concentration in the y direction, corresponding with the images in Fig. 1, are blunted due to the higher stress generated in the z direction. The concentration profile at $\phi_{\text{bulk}}=0.1$ does show a slight drift of particles in the z direction, likely due to the density mismatch of the fluid and particles. No significant recirculation in the transverse direction results from this subtle drift.

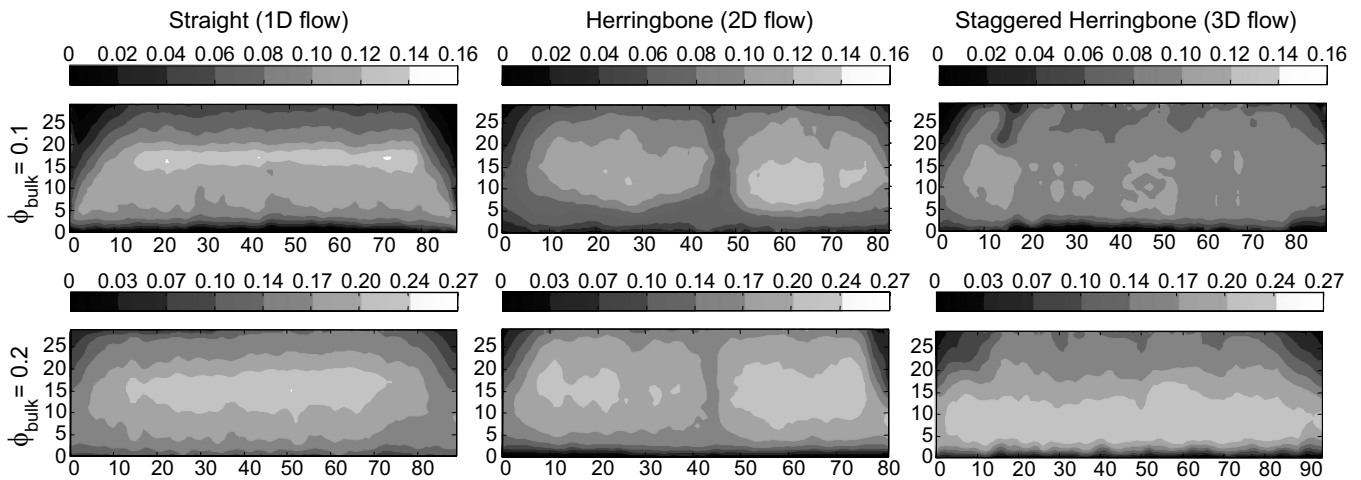


FIG. 2. The concentration profiles in the transverse direction to the pressure-driven flow for both $\phi_{bulk} = 0.1$ and 0.2 in 1D, 2D, and 3D flows show the interplay between shear-induced migration and the underlying flow. Axes scales are in μm .

In 2D flows for both $\phi_{bulk}=0.1$ and 0.2 , the two concentrated bands are clear, each located away from the side and top and bottom walls, roughly outlining the recirculation regions in the transverse direction to flow. The particle-depleted region in the center has a lower concentration than bulk, demonstrating that particle migration results in a net flux away from the center of the channel. The maximum concentration found in the two axial bands is similar to that observed in the 1D flow, suggesting that the recirculation does not mitigate shear migration. The concentration profiles of each band are asymmetric, suggesting that the initial migration of particles is nonuniform. As was found in the 1D flow, the maximum concentration is located lower than center in the z direction due to mismatched buoyancy of the fluid and particles. In contrast to the 1D flow where interactions in the segregated band are almost purely diffusive, particles in the segregated bands formed by 2D flows have significant recirculation, enhancing overall transport, yet still resulting in significant concentration gradients.

The concentration profiles generated by 3D flows at $\phi_{bulk}=0.1$ and 0.2 differ greatly from each other and from what may be expected. At $\phi_{bulk}=0.1$, distinct bands are not clear and the overall concentration profile is more uniform. The region where particle-depleted fluid near the top left of the cross section is evident; however, its effect on the overall concentration appears to be quickly dissipated. A few small regions having slightly higher concentrations of a maximum $\phi=0.129$, less than that found in 1D and 2D flows. It appears that mixing in this geometry does mediate the effects of shear-induced migration. In contrast, at $\phi_{bulk}=0.2$ the segregation profile is more similar to the profile generated in 1D channels forming a single concentrated band. This profile does not demonstrate any of the finer structures expected to be generated by the flow, and the single concentrated band has a maximum concentration of $\phi=0.274$ that dominates the profile, showing that this 3D flow results in the same degree of segregation as in 1D and 2D flows. More accurately, it is unclear whether 3D convection is generated in the concentrated suspension; flow in the transverse direction is strongly damped. The band is located near the bottom wall,

which suggests that either the recirculation in the transverse direction enhanced the particle-fluid buoyancy mismatch or the HBs enhanced shear migration downward during the development of this final concentration profile.

The observations presented thus far can be summarized as follows. In systems having closed, integrable streamlines, shear-induced migration is largely unchecked and the introduction of chaotic advection does in part mediate the effects of particle migration at low concentration. In general, shear migration dominates these flows although it is typically seen as relatively weak and its rate as collisional diffusion limited. This weak effect does integrate over time, and the interplay with the underlying flow is highly complex. Because different regions of the flow can be characterized as particle rich and particle depleted, there are remaining questions regarding the stability of these flows and structures. Observations near the entrance region of the 2D flow, shown in Fig. 3, depict a yet more complicated view of the evolution of these structures. The early recirculation driven by the HBs injects a low concentration, and therefore a lower viscosity, fluid into the center of the suspension. This results in a spatiotemporal jet buckling resulting from a linear Kelvin-Helmholtz instability [30,31]. The buckle in the concentration slowly waves left and right over a period much longer than the scanning

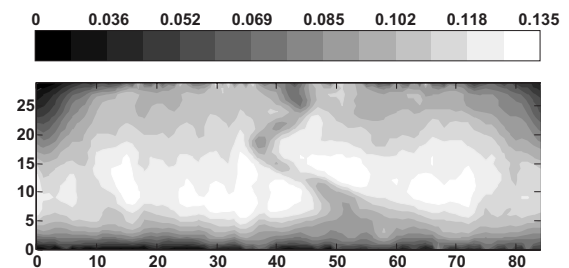


FIG. 3. The concentration profile near the entrance of the channel, after the first six symmetric HBs, demonstrates a Kelvin-Helmholtz instability at $\phi_{bulk} = 0.1$. Fluid of lower particle concentration near the walls buckles as it is injected into the bulk of the suspension. Axes scales are in μm .

rate. The onset of this instability depends on the concentration mismatch and the recirculation, both of which depend on the degree of shear migration.

In summary, the interplay between ordering via migration and topologically complex flows is highly complicated, where shear-induced migration is not simply mediated by inducing chaotic advection. Furthermore, instabilities arising during the onset of migration in these flows limit the possibility of using segregation as a tool for developing separation processes without significant consideration of the suspension properties and operating parameters of these systems. Furthering our understanding of this interplay promises to allow

significant developments in “lab-on-a-chip” unit operations, predicting dispersion in large-scale processes, and a quantitative description of complicated natural processes, and will be the basis of ongoing research focusing on these systems.

We thank J. Morris and J. Brady for insightful conversations on suspension transport, and E. Weeks for discussions regarding microfluidics and confocal microscopy. The micro-fabrication was performed at the Cornell NanoScale Facility, and this material is based upon work supported by the National Science Foundation under Grant No. 0630191 and funding from the ACS Petroleum Research Fund.

-
- [1] D. Leighton and A. Acrivos, *J. Fluid Mech.* **181**, 415 (1987).
 [2] P. Nott and J. Brady, *J. Fluid Mech.* **275**, 157 (1994).
 [3] M. Lyon and L. Leal, *J. Fluid Mech.* **363**, 25 (1998).
 [4] C. Koh, P. Hookham, and L. Leal, *J. Fluid Mech.* **266**, 1 (1994).
 [5] M. Frank *et al.*, *J. Fluid Mech.* **493**, 363 (2003).
 [6] R. Hampton *et al.*, *J. Rheol.* **41**, 621 (1997).
 [7] A. Averbakh *et al.*, *Int. J. Multiphase Flow* **23**, 409 (1997).
 [8] J. Butler and R. Bonnecaze, *Phys. Fluids* **11**, 1982 (1999).
 [9] J. Abbott *et al.*, *J. Rheol.* **35**, 773 (1991).
 [10] R. Phillips *et al.*, *Phys. Fluids A* **4**, 30 (1992).
 [11] A. Chow *et al.*, *Phys. Fluids* **6**, 2561 (1994).
 [12] N. Tetlow *et al.*, *J. Rheol.* **42**, 307 (1998).
 [13] J. Iwamiya, A. Chow, and S. Sinton, *Rheol. Acta* **33**, 267 (1994).
 [14] S. Altobelli, E. Fukushima, and L. Mondy, *J. Rheol.* **41**, 1105 (1997).
 [15] T. Moraczewski, H. Tang, and N. Shapley, *J. Fluid Mech.* **49**, 1409 (2005).
 [16] N. Phan-Thien *et al.*, *Ind. Eng. Chem. Res.* **34**, 3187 (1995).
 [17] S. Subia *et al.*, *J. Fluid Mech.* **373**, 193 (1998).
 [18] J. Ritz *et al.*, *Chem. Eng. Sci.* **55**, 4857 (2000).
 [19] A. Leshansky, A. Bransky, N. Korin, and U. Dinnar, *Phys. Rev. Lett.* **98**, 234501 (2007).
 [20] R. M. Jendrejack, E. T. Dimalanta, D. C. Schwartz, M. D. Graham, and J. J. de Pablo, *Phys. Rev. Lett.* **91**, 038102 (2003).
 [21] J. Moger *et al.*, *J. Biomed. Opt.* **9**, 982 (2004).
 [22] J. Ottino, *The Kinematics of Mixing* (Cambridge University Press, Cambridge, England, 1989).
 [23] J. Ottino and S. Wiggins, *Philos. Trans. R. Soc. London, Ser. A* **362**, 923 (2004).
 [24] A. Stroock *et al.*, *Science* **295**, 647 (2002).
 [25] Y. Xia and G. Whitesides, *Annu. Rev. Mater. Sci.* **28**, 153 (1998).
 [26] A. Sierou and J. Brady, *J. Rheol.* **46**, 1031 (2002).
 [27] A. Ramachandran and D. Leighton, *Phys. Fluids* **19**, 053301 (2007).
 [28] Concentration profiles measured at $\frac{L}{H}=1500$ and 2000 confirm that the profile is steady.
 [29] Concentration profiles are generated from six columns of image stacks, each representing $21 \times 21 \times 32 \text{ mm}^3$, via confocal microscopy (vteye, VisiTech International). Data are averaged over nine total scans, each taken at 170 fps to reduce distortions related to velocity in the z direction in 2D and 3D flows. The locations of over 150 000 individual particles, determined by using the IDL code developed by Eric Weeks at Emory University using algorithms developed by Crocker and Grier [32], are binned to represent local concentration and verify ϕ_{bulk} .
 [30] W. Thomson, *Philos. Mag.* **42**, 362 (1871).
 [31] H. von Helmholtz, *Philos. Mag.* **4**, 337 (1868).
 [32] J. Crocker and D. Grier, *J. Colloid Interface Sci.* **179**, 298 (1996).